IEEE Access
Multidisciplinary : Rapid Review : Open Access Journal

Received 21 June 2023, accepted 28 July 2023, date of publication 31 August 2023, date of current version 13 September 2023.

Digital Object Identifier 10.1109/ACCESS.2023.3310823

RESEARCH ARTICLE

Analysis of Logic-in-Memory Full Adder Circuit With Floating Gate Field Effect Transistor (FGFET)

SUEYEON KIM[1], INSOO CHOI[1], SANGKI CHO[1], MYOUNGGON KANG[2], (Senior Member, IEEE), SEUNGJAE BAIK[3], CHANGHO RA[4], AND JONGWOOK JEON[4]

[1]Department of Electrical and Electronics Engineering, Konkuk University, Seoul 05029, South Korea
[2]Department of Electronics Engineering, Korea National University of Transportation, Chungju-si 27469, South Korea
[3]Semiconductor Research and Development Center, Samsung Electronics, Hwasung-si 18448, South Korea
[4]School of Electronic and Electrical Engineering, Sungkyunkwan University, Suwon-si 16419, South Korea

Corresponding authors: Changho Ra (wocwoc3@gmail.com) and Jongwook Jeon (voix0707@skku.edu)

This work was supported in part by the National Research and Development Program through the National Research Foundation of Korea (NRF) funded by the Ministry of Science and ICT under Grant 2021M3F3A2A03017693, and in part by IC Design Education Center (IDEC).

ABSTRACT The high data throughput and high energy efficiency required recently are increasingly difficult to implement due to the von Neumann bottleneck. As a way to overcome this, Logic-in-Memory (LiM) technology has recently been receiving a lot of attention. In particular, since the addition function is important to solve high data throughput in applications such as artificial intelligence, the results of applying various fine-grain LiM application devices to full adder circuit design are being announced. In this paper, a Floating Gate Field Effect Transistor (FGFET), which has a structure similar to a floating gate memory cell transistor that has been widely used in the past and is highly applicable to mass production, was applied to the LiM application circuit design. Prior to application to circuit design, the FGFET characteristics were confirmed using a well-calibrated technology computer-aided design (TCAD) simulation at the 32nm technology node, and a compact model was developed to describe them. Afterwards, the delay and power consumption were evaluated with three different types of FGFET-based full adder circuits, and benchmarked with conventional CMOS (complementary metal-oxide-semiconductor)-based conventional full adder circuits.

INDEX TERMS von Neumann bottleneck, logic-in-memory, floating gate field effect transistor (FGFET), full adder, compact modeling.

I. INTRODUCTION

The von Neumann architecture is a structure in which the CPU (Central Processor Unit) and memory are separated, and data transmission is performed through the system bus. Recently, as artificial intelligence, big data, and cloud computing applications develop, computer architecture tends to change from 'Computing-intensive' to 'Memory-intensive'. At this time, it is becoming increasingly difficult to satisfy the requirements for such applications with the traditional von Neumann architecture, due to a phenomenon called 'Memory wall' or 'von Neumann bottleneck' [1], [2]. Logic-in-Memory technology is attracting attention as a way to overcome this problem [1], [3], [4]. The core of LiM technology is to increase the efficiency of data transfer by placing the memory and the processing unit close together without separating them, and it can be classified in various ways according to the location of processor and memory within the computer architecture [5]. Recently, various non-volatile memory technologies have been studied as LiM technologies are being announced [6], [7], [8], [9].

In particular, since the addition function is important in applications such as artificial intelligence, the results of applying various existing fine-grain LiM application devices to full adder circuit design have been announced [10], [11], [12], [13], [14]. Comparison between a full adder consisting of an existing silicon CMOS transistor and a fine-grain LiM transistor (e.g. FeFET) shows superior circuit area and

The associate editor coordinating the review of this manuscript and approving it for publication was Paolo Crippa.

This work is licensed under a Creative Commons Attribution-NonCommercial-NoDerivatives 4.0 License. For more information, see https://creativecommons.org/licenses/by-nc-nd/4.0/

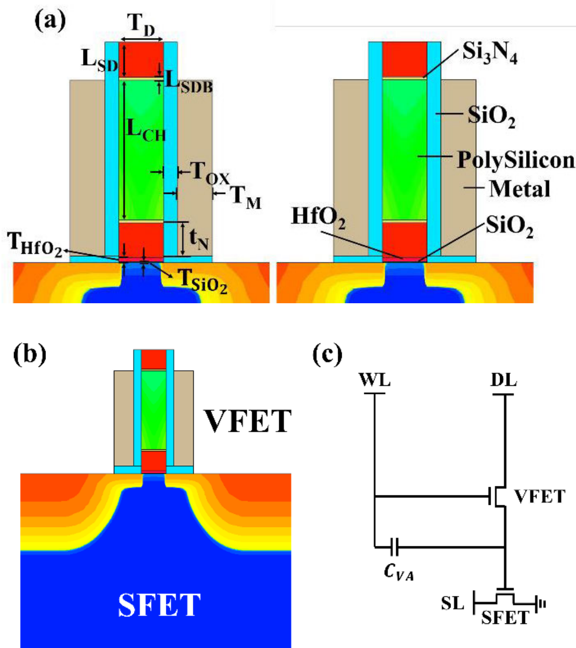

FIGURE 1. (a) Cross-section view of FGFET (b) FGFET Structure with SFET and VFET (c) Equivalent circuit describing FGFET device which includes SFET, VFET and coupling capacitance.

energy consumption characteristics, confirming the possibility of applying LiM transistor technology to a new computer architecture.

This work intends to show the LiM technology based on the FGFET structure, whose integration with the CMOS FET is much better than the aforementioned LiM non-volatile devices, since it is based on the floating memory technology used in the existing silicon-based NAND flash memory. The FGFET structure is based on the device structure named STTM (Scalable Two Transistor Memory) and PLEDM (Phase-state Low Electron-number Drive Random Access Memory) announced by Samsung Electronics and Hitachi [15], [16], [17], [18], [19], [20]. The floating node that stores the data is placed on the gate stack of a general MOSFET, and the data writing function is performed by applying the data line voltage (V_{DL}) and the word line voltage (V_{WL}). In this work, FGFET is applied to the most scaled-down 32nm technology node in the single gate planar MOSFET logic process to show LiM device characteristics, develop a compact model for FGFET that can be described in a circuit simulator, and perform various full adder circuit analyzes that is applied LiM technology. Two of the total three full adder circuits utilized the scheme of the previous thesis, and one is a newly proposed circuit in this work. In addition, the FGFET-based full adder circuit shows the result of benchmarking the silicon-based full adder and circuit characteristics of the existing 32nm technology node.

This paper is structured as follows. Chapter 2 describes the FGFET device structure and compact model. Next, Chapter 3 includes the results of optimizing the voltage conditions

TABLE 1. Values for key device parameters of FGFET in this work.

Parameters	Values
Gate separation (T_D)	32nm
VFET Gate Oxide Thickness (T_{OX})	10nm
Metal Thickness (T_M)	25nm
VFET Channel Length (L_{CH})	100.2nm
Source/Drain Length (L_{SD})	25nm
Source/Drain Barrier (L_{SDB})	2nm
VFET Channel Doping	Intrinsic
VFET S/D Doping	$2\cdot10^{20}cm^{-3}$
Memory Node Thickness (t_N)	23.7nm
SiO_2 Thickness (T_{SiO_2})	0.7nm
HfO_2 Thickness (T_{HfO_2})	3nm
Substrate Doping	$1\cdot10^{16}cm^{-3} \sim 1.8\cdot10^{17}cm^{-3}$
SFET Source/Drain Doping	$5\cdot10^{19}cm^{-3}$

in various full-adder circuit schemes by using the developed model library for FGFET, and benchmarking with the silicon CMOS technology. Finally, we would like to conclude and end in chapter 4.

II. OPERATION AND COMPACT MODELING OF FGFET

In this chapter, the structure and operation principle of the FGFET device, and compact model with well calibrated TCAD data as reference are explained. The FGFET structure is composed of vertical FET (VFET) and sense FET (SFET) as shown in Fig.1(b). The source of the VFET and the gate of the SFET meet to form a memory node, and a coupling cap is generated during integration into the FGFET structure.

In this study, the 32nm planar MOSFET, which is the node just before the FinFET structure was applied, was selected as the SFET that serves as the baseline for FGFET referring to the ITRS roadmap and Predictive Technology Model (PTM). In the case of VFET, the channel length (L_{CH}) was set considering the aspect ratio of the fabricated FGFET, which has been presented in previous papers [21], [22]. The key design parameters of the FGFET are summarized in Fig.1(a) and Table 1, and the FGFET is analyzed using commercial TCAD software. Synopsys' Sentaurus^{TM} was used as commercial TCAD, and drift-diffusion and tunneling mechanisms are important to verify the electrical characteristics of FGFET. Calibration was performed with related transport model parameters by using measurement data of the VFET fabricated, and well-known target characteristics at the 32nm technology node. In this way, the electrical characteristics (I-V, C-V) of the FGFET were predicted by using the well-calibrated TCAD, and a compact model describing them was produced.

Fig.1(c) is the equivalent circuit of FGFET, SFET and VFET are implemented as an industry standard BSIM4 model, and the coupling cap component generated in the

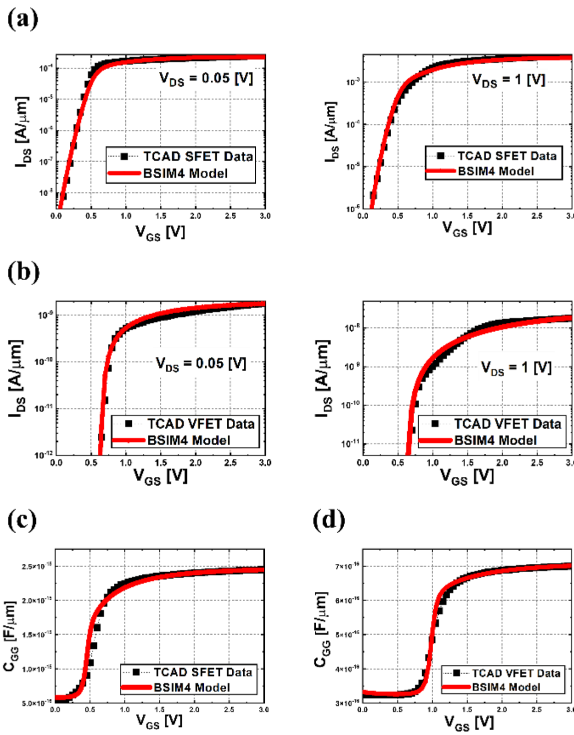

FIGURE 2. (a) SFET log plot: $I_d V_g @V_{DS} = 50mV, 1V$ (b) VFET log plot: $I_d V_g @V_{DS} = 50mV, 1V$ (c) SFET C-V curve (d) VFET C-V curve.

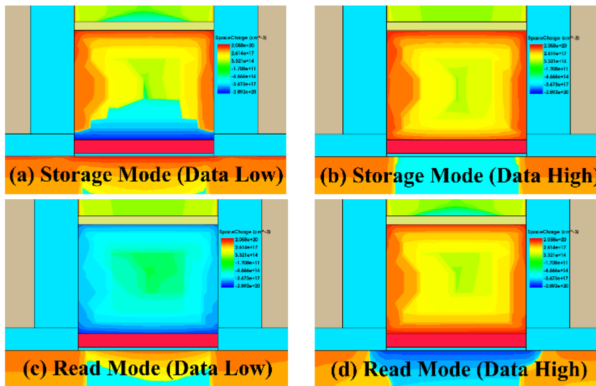

FIGURE 3. Space charge density profile at memory node of FGFET under (a) storage mode (Data low) (b) storage mode (Data high) (c) read mode (Data low) (d) read mode (Data high).

integration process is implemented with verilog-a language [23]. The VFET and SFET electrical characteristic curves obtained from TCAD were developed through the BSIM4 model library, and it can be confirmed that the developed model library accurately describes the electrical characteristics of SFET and VFET individual devices as shown in Fig.2.

After the development of individual SFET and VFET model libraries, the coupling capacitance (C_{VA}), which varies depending on the voltage condition applied to the VFET, was modeled by using verilog-a. After that, the integrated FGFET model was developed by connecting C_{VA} between SFET and VFET as shown in Fig.1(c). Fig.3(a)-(b) shows the charge

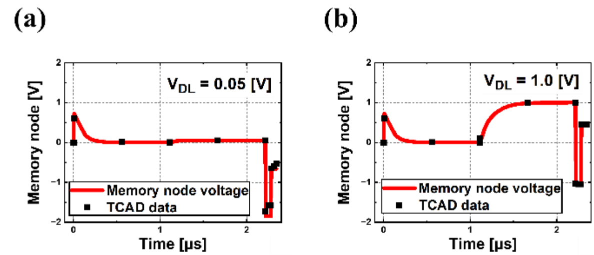

FIGURE 4. (a) Transient result for data low ($V_{DL} = 0.05V$ (b) Transient result for Data High ($V_{DL} = 1V$).

TABLE 2. Voltage conditions for FGFET operation modes.

Mode	WL [V]	DL [V]	SL [V]
Initialize	3	0	0
Write	3	Low(0.05) / High(1)	0
Storage	-2	0	0
Read	0.5	0	0.9

distribution extracted by using TCAD in the storage mode where the word line voltage (V_{WL}) is -2V and the data line voltage (V_{DL}) and the sense line voltage (V_{SL}) are both 0V. Fig.3(c)-(d) shows the charge distribution in the read mode where word line voltage (V_{WL}) is 0.5V, data line voltage (V_{DL}) is 0V, and sense line voltage (V_{SL}) is 0.9V. When data is low, 0.05V is applied through the data line in the write mode, and when data is high, 1V is applied through the data line in write mode. At this time, it can be confirmed through Fig.3 that the coupling capacitance should consider not only the physical cap by the dielectric layer but also the depletion cap that varies depending on the voltage condition.

The operation modes of FGFET varies depending on the voltage applied to the word line and data line. The initialize mode applies 3V to the word line, does not apply voltage to the data line and sense line, and initializes the memory node voltage (V_{MN}) to 0V before writing the data. The write mode applies 3V to the word line and 0V to the sense line, and applies 1V to the data line when writing '1' and 0.05V when writing '0'. In this step, the data of V_{MN} is determined by the voltage applied to the data line, and the current flowing through the SFET is determined, so it can function as a memory cell. After that, the storage mode is performed in which -2V is applied only to the word line while 0V is applied to the data line and the sense line. Through this process, the data of the memory node is not volatilized until the read mode, implementing the non-volatile function of FGFET. After the storage mode, the data of the memory node is read by applying 0.9V to the sense line and 0.5V to the word line. If '1' is written in the write process, the SFET is turned on and current flows, and if '0' is written, the SFET is not turned on and current does not flow, so the written data can be checked

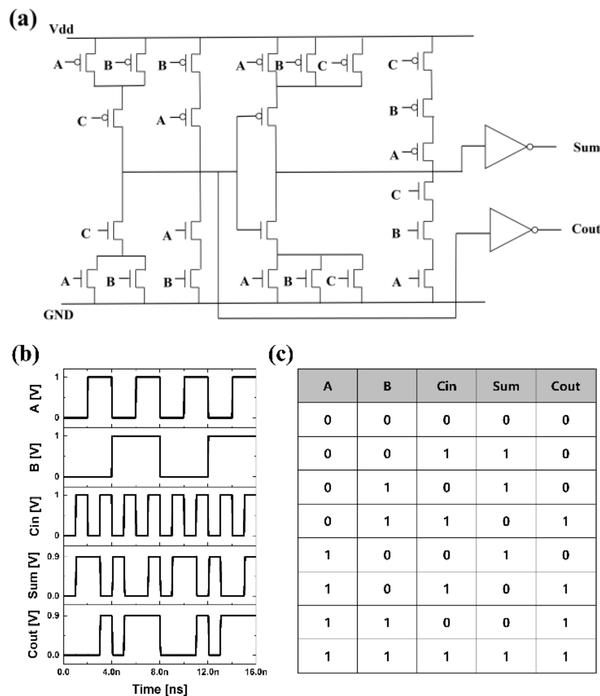

A	B	Cin	Sum	Cout
0	0	0	0	0
0	0	1	1	0
0	1	0	1	0
0	1	1	0	1
1	0	0	1	0
1	0	1	0	1
1	1	0	0	1
1	1	1	1	1

FIGURE 5. (a) Conventional 28FET full adder circuit (b) Timing graph (c) Logic table.

accurately. The applied voltage conditions according to the operation modes are summarized in Table 2, and the transient characteristics of the FGFET in various operation modes can be described with the developed compact model as shown in Fig.4.

III. FULL ADDER DESIGN BASED ON FGFET

A. CONVENTIONAL 28FET FULL ADDER

Full adder is a logic circuit that calculates a single digit of a binary number and outputs it by adding a lower digit number input. Fig.5(c) shows the truth table of full adder. In order to benchmark the FGFET-based full adder with the conventional 28FET full adder, the performance of the conventional 28FET full adder was checked using the CMOS FET of the 32nm technology node. Note that the CMOS FET of the 32nm technology node has the same electrical characteristics as the SFET of the FGFET. The space efficiency was compared through the number of transistors used in the circuit configuration and layout area. The operating performance was compared by measuring dynamic power, static power, delay, and PDP. PDP is a product of delay and dynamic power.

The conventional full adder is a circuit using a total of 28 baseline FETs as shown in Fig.5(a). The delay was measured as a 1-bit delay, which is the time it takes for the output of the upper carry number (Cout) of the full adder to be calculated after the lower carry number (Cin) is entered when '0'+'1' is calculated. As a result, dynamic power was measured as 1.14uW, static power as 16.51nW, and delay as 44.55ps. In addition, PDP, which is a key indicator of the operation performance of the full adder, was measured at 50.79aW·s. Fig.9(a) is a conventional 28FET full adder layout, which was designed according to the 32nm layout design rules of the ITRS roadmap [24]. Two metal layers were used and the total area was 3.75um^2.

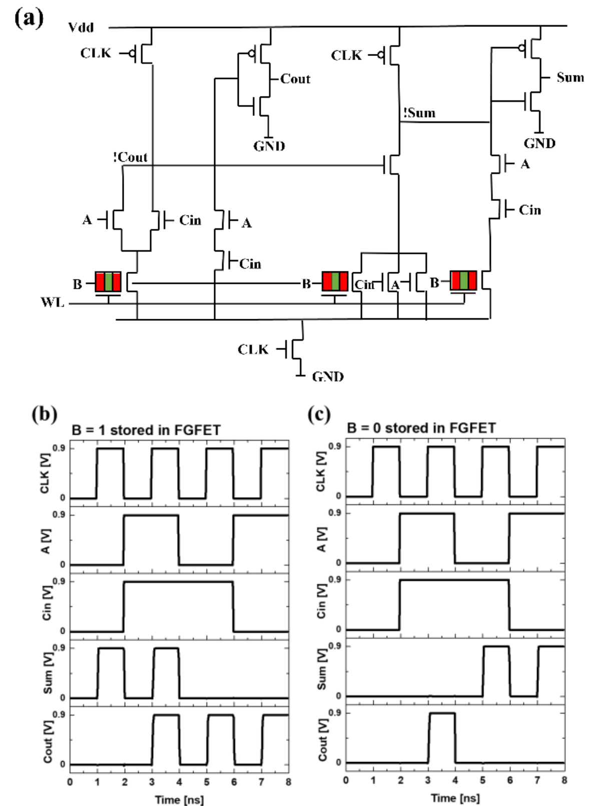

FIGURE 6. (a) A-type full adder based on FGFET circuit (b) Timing graph (B = 1 stored in FGFET) (c) Timing graph (B = 0 stored in FGFET).

B. FGFET-BASED FULL-ADDER A-TYPE

The FGFET-based full adder A-type (hereinafter referred to as A-type) is a full adder circuit composed of NMOS except for the clock transistor and inverter transistor as shown in Fig.6(a). A-type is a full adder circuit proposed using [13]. Since 19 transistors (16FET + 3FGFETs) are used, which is 9 fewer than the conventional 28FET full adder, there is a clear advantage over the existing circuit in terms of space efficiency. The area efficiency can also be confirmed in Fig.9(b), which is an A-type layout. A-type uses 4 metal layers, and the total area is 2.46um^2, which reduces 34.4% compared to the conventional full adder.

A-type uses the memory node voltage as input B, and the current of the SFET is determined by the memory node voltage. At this time, 1.9V was applied to the data line when writing '1' and 0.05V was applied to the data line when writing '0'. The word line voltage applied in the write mode is 3V, which is the same as the initialize mode. After writing, -2V was applied to the word line to proceed with the storage mode. Afterwards, the data written in the memory node was

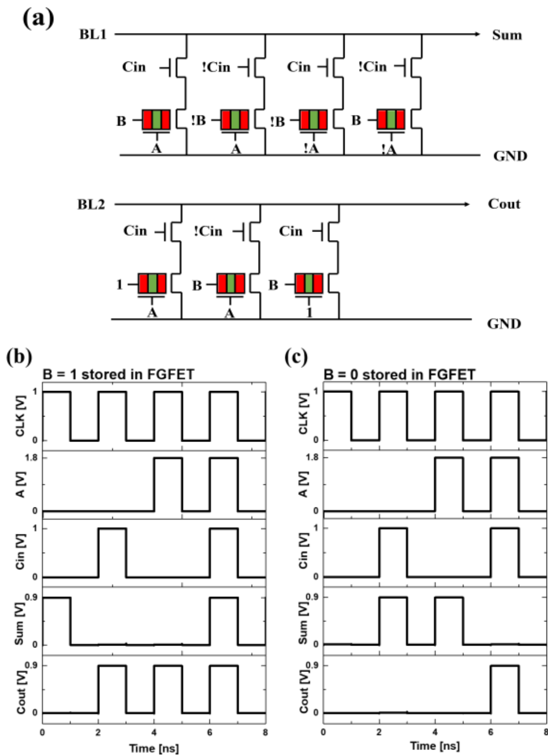

FIGURE 7. (a) B-type full adder based on FGFET circuit (b) Timing graph (B = 1 stored in FGFET) (c) Timing graph (B = 0 stored in FGFET).

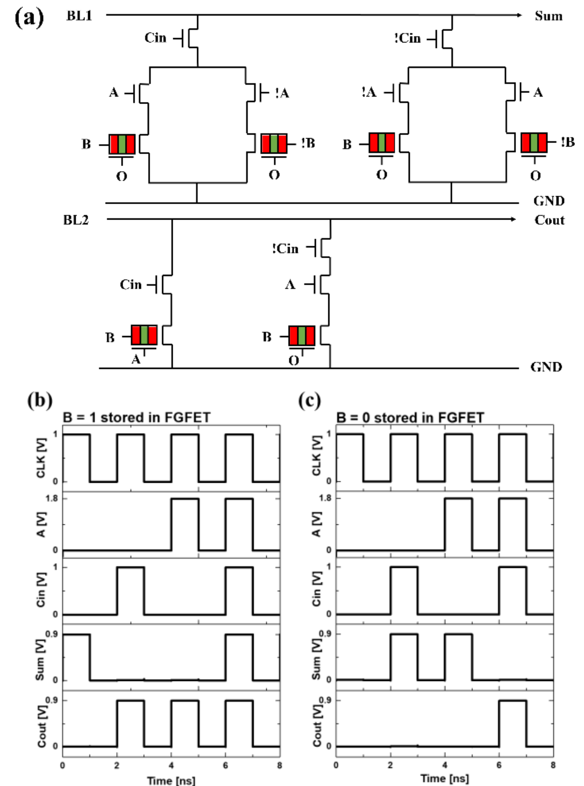

FIGURE 8. (a) C-type full adder based on FGFET circuit (b) Timing graph (B = 1 stored in FGFET) (c) Timing graph (B = 0 stored in FGFET).

read by applying a read voltage of 0.5V to the word line in the same way as the memory operating condition. During the read operation, if '1' is written during the write process, the SFET is turned on and current flows, and if '0' is written, the SFET is not turned on and current does not flow. When the read voltage is applied to the FGFET, pulses corresponding to the input A and input Cin are applied to the other baseline FET gate to check the logic operation and measure the dynamic power, static power, delay, and PDP.

As a result, the dynamic power showed the same performance as the conventional 28FET full adder at 1.14uW, although the number of elements was reduced.

This is the effect of leakage current that occurs when the transistor connected to the !Cout node is not immediately turned off while the current flow is instantaneously changed by the operation of the clock transistor. The static power is 13.64nW, which reduces the number of elements constituting the entire circuit, and reduces the leakage current due to the GIDL phenomenon by the Si_3N_4 barrier inserted between the source/drain and channel. Therefore, it decreased to 82.62% level compared to the conventional 28FET full adder. Also, the delay was measured as 43.54ps and slightly decreased to 97.73% of the existing 28FET full adder. As a result, the PDP is slightly reduced to 49.64aW·s, which is 97.73% of the conventional 28FET full adder, and has an advantage in terms of operating performance compared to the conventional 28FET full adder.

C. FGFET-BASED FULL-ADDER B-TYPE

In the case of FGFET-based full adder B-type (hereinafter referred to as B-type), the FeFET full adder of the array structure proposed in the Evelyn T.Breyer paper is a circuit implemented with FGFET as shown in Fig.7(a). [14] A total of 20 transistors (13FET+7FGFET) are used, including 2 pull-up clock transistors connected to the bit line and 4 inverter transistors for Sum and Cout outputs, which is 8 fewer than the conventional 28FET full adder. Also, B-type differs from A-type in that it is a structure in which Sum and Cout are independently operated. Fig.9(c) is a B-type layout where 4 metal layers are used and the total area is 2.24um^2, reducing 40.3% compared to the conventional full adder.

The biggest feature of the B-type operation principle is that input A and input B are applied as read voltage and write voltage of FGFET, respectively, and FGFET operates with AND gate as shown in Fig.7(b). That is, '1' is output only when the read voltage, which is the voltage applied to the word line in read mode, and the write voltage, which is the voltage applied to the data line in write mode, are both '1'. The read voltage was set as input A, and 1.8V was applied for '1' and 0V for '0' through the word line in read mode. The write voltage was set to input B as in A-type, and 1.8V for '1' and 0.1V for '0' were applied through the data line in write mode. Afterwards, since the current should flow through the

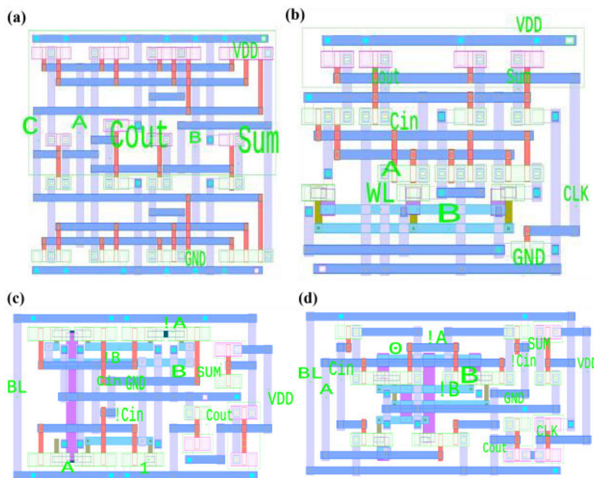

FIGURE 9. (a) Conventional 28FET full adder layout (b) FGFET-based full adder A-type layout (c) FGFET-based full adder B-type layout (d) FGFET-based full adder C-type layout.

TABLE 3. Performance and power of full adders.

Device	Transistor Count	V_{DD} [V]	T_D [ps]	P_{DYN} [μW]	P_{static} [nW]	PDP [W·s]	Area [μm^2]
Conventional 28FET FA	28FET	0.9	44.55	1.14	16.51	50.79e^{-18}	3.75
FGFET FA A-type	16FET+ 3FGFETs	0.9	43.54	1.14	13.64	49.64e^{-18}	2.46
FGFET FA B-type	13FE T + 7FGFETs	0.9	41.25	1.08	5.37	44.55e^{-18}	2.24
FGFET FA C-type	15FET + 6FGFETs	0.9	16.44	0.93	5.55	15.29e^{-18}	2.53

SFET of the FGFET only when both the read voltage and the write voltage are '1', the threshold voltage value was shifted 0.9V by using the DELVT0 parameter value.

After going through initialize, write, and storage modes in the same way as A-type, pulses were applied to the baseline FET in read mode to compare static power, dynamic power, delay, and PDP. First, the dynamic power was measured at 1.08uW, which was reduced to 94.74% compared to the conventional 28FET full adder. This is due to the reduced number of circuit components compared to the conventional 28FET full adder. However, unlike the A-type, the B-type has clearly improved dynamic power performance because the Sum and Cout circuits are configured independently, so leakage due to switching does not occur. Static power is measured as 5.40nW due to the reduced GIDL leakage current by the Si_3N_4 barrier and the reduced number of circuit components, similar to the A-type. This is greatly reduced to the level of 32.53% compared to the conventional 28FET full adder. In the case of delay, due to the simple circuit configuration of the array structure, it is measured as 41.25ps and reduced to 92.59% compared to the conventional 28FET full adder. As a result, the PDP was reduced to 44.55aW·s, which is 87.71% compared to the existing conventional 28FET full adder, showing a clear advantage in terms of operating performance.

D. FGFET-BASED FULL-ADDER C-TYPE

The FGFET-based Full Adder C-type (hereafter C-type) proposed for the first time in this work does not move the threshold voltage unlike the B-type. Also, in C-type, FGFET is characterized by operating as an OR gate as shown in Fig.8(b). Therefore, in the case of C-type, if the read voltage or write voltage is '1', output comes out '1'. Also, unlike B-type, there are cases where input A is used as the read voltage of FGFET and case where it is used as baseline FET gate voltage. The C-type circuit is shown in Fig.8(a), and the total number of transistors is 21 (15FET + 6FGFET), including 2 pull-up clock transistors connected to bit lines and 4 inverter transistors for Sum and Cout. The C-type is 7 fewer than the conventional 28FET full adder. Also Fig.9(d) is a C-type layout, 4 metal layers were used, and the total area was 2.53um^2, which was reduced by 32.5% compared to the conventional full adder, confirming the efficiency in terms of area.

As for the voltage condition, in the case of input A applied as a read voltage through the word line in FGFET read mode, 1.2V is applied for '1' and 0V for '0'. In the case of input A applied to the baseline FET, 1V was applied for '1' and 0V for '0', the same as other baseline FET gate voltages. The write voltage corresponding to input B was 1.85V when it was '1' and 0.85V when it was '0' in write mode. Afterwards, static power, dynamic power, delay, and PDP were measured as the same way as A-type and B-type.

As with the B-type, the dynamic power was reduced to 0.93uW, 81.58% of the conventional 28FET full adder, due to the decrease in the number of circuit elements. Similar to the FGFET-based full adder mentioned earlier, the static power dropped significantly to 5.55 nW, a 33.62% level, due to the reduced number and reduced GIDL leakage current applied to the barrier. In the case of delay, as in the B-type, due to the circuit configuration of the array structure, 16.44 ps was significantly reduced to 36.90% compared to the conventional 28FET full adder. As a result, the PDP expressed as the product of dynamic power and delay was 15.29aW·s, which was reduced by 30.10% compared to the conventional 28FET full adder.

IV. CONCLUSION

In this work, the FGFET device that can be used for next-generation LiM applications is introduced and applied to the 32nm planar MOSFET technology node for the first time to show the LiM full adder circuit design characteristics. To this end, the structure and operating principle of the FGFET are explained, and the performance of three different types of full adder circuits based on FGFET is verified by using the FGFET compact model.

All three full adders show a great advantage compared to the conventional 28FET full adder in terms of static power due to the Si_3N_4 barrier structure inserted between source/drain and channel. In addition, as the number of elements constituting the circuit decreased, not only the advantage in terms of space efficiency, but also improved indicators in PDP, an indicator related to operating performance. As such, FGFET, which has been confirmed to be applicable to LiM application circuits, has a structure similar to silicon-based floating gate memory cell transistors that have been widely used in the past, so it is very likely to be applied to mass production. Therefore, it is a device technology that is highly likely to be applied to mass production in the industry in the future.

ACKNOWLEDGMENT

(Sueyeon Kim and Insoo Choi contributed equally to this work.)

REFERENCES

[1] X. Huang, C. Liu, Y.-G. Jiang, and P. Zhou, "In-memory computing to break the memory wall," *Chin. Phys. B*, vol. 29, no. 7, Jul. 2020, Art. no. 078504.

[2] W. A. Wulf and S. A. McKee, "Hitting the memory wall: Implications of the obvious," *ACM SIGARCH Comput. Archit. News*, vol. 23, no. 1, pp. 20–24, Mar. 1995.

[3] O. Mutlu, S. Ghose, J. Gómez-Luna, and R. Ausavarungnirun, "Processing data where it makes sense: Enabling in-memory computation," *Microprocessors Microsyst.*, vol. 67, pp. 28–41, Jun. 2019.

[4] A. Sebastian, M. L. Gallo, R. Khaddam-Aljameh, and E. Eleftheriou, "Memory devices and applications for in-memory computing," *Nature Nanotechnol.*, vol. 15, no. 7, pp. 529–544, Jul. 2020.

[5] I. O'Connor, M. Cantan, C. Marchand, B. Vilquin, S. Slesazeck, E. T. Breyer, H. Mulaosmanovic, T. Mikolajick, B. Giraud, J.-P. Noël, A. Ionescu, and I. Stolichnov, "Prospects for energy-efficient edge computing with integrated HfO_2-based ferroelectric devices," in *Proc. IFIP/IEEE Int. Conf. Very Large Scale Integr. (VLSI-SoC)*, Oct. 2018, pp. 180–183.

[6] N. Talati, R. Ben-Hur, N. Wald, A. Haj-Ali, J. Reuben, and S. Kvatinsky, "mMPU—A real processing-in-memory architecture to combat the von Neumann bottleneck," in *Applications of Emerging Memory Technology*. Singapore: Springer, 2020, pp. 191–213.

[7] D. Ielmini and H.-S.-P. Wong, "In-memory computing with resistive switching devices," *Nature Electron.*, vol. 1, no. 6, pp. 333–343, Jun. 2018.

[8] X. Chen, X. Yin, M. Niemier, and X. S. Hu, "Design and optimization of FeFET-based crossbars for binary convolution neural networks," in *Proc. Design, Autom. Test Eur. Conf. Exhib. (DATE)*, Mar. 2018, pp. 1205–1210.

[9] Y. Zhang, L. Xu, K. Yang, Q. Dong, S. Jeloka, D. Blaauw, and D. Sylvester, "Recryptor: A reconfigurable in-memory cryptographic cortex-M0 processor for IoT," in *Proc. Symp. VLSI Circuits*, Jun. 2017, pp. C264–C265.

[10] T. Zanotti, F. M. Puglisi, and P. Pavan, "Smart logic-in-memory architecture for low-power non-von Neumann computing," *IEEE J. Electron Devices Soc.*, vol. 8, pp. 757–764, 2020, doi: 10.1109/JEDS.2020.2987402.

[11] P. Barla, V. K. Joshi, and S. Bhat, "Design and evaluation of a self write-terminated hybrid MTJ/CMOS full adder based on LIM structure," *J. Circuits, Syst. Comput.*, vol. 31, no. 8, May 2022, Art. no. 2250146.

[12] C. Marchand, I. O'Connor, M. Cantan, E. T. Breyer, S. Slesazeck, and T. Mikolajick, "FeFET based logic-in-memory: An overview," in *Proc. 16th Int. Conf. Design Technol. Integr. Syst. Nanosc. Era (DTIS)*, Jun. 2021, pp. 1–6, doi: 10.1109/DTIS53253.2021.9505078.

[13] X. Yin, A. Aziz, J. Nahas, S. Datta, S. Gupta, M. Niemier, and X. Sharon Hu, "Exploiting ferroelectric FETs for low-power non-volatile logic-in-memory circuits," in *Proc. IEEE/ACM Int. Conf. Comput.-Aided Design (ICCAD)*, Nov. 2016, pp. 1–8, doi: 10.1145/2966986.2967037.

[14] E. T. Breyer, H. Mulaosmanovic, J. Trommer, T. Melde, S. Dunkel, M. Trentzsch, S. Beyer, S. Slesazeck, and T. Mikolajick, "Compact FeFET circuit building blocks for fast and efficient nonvolatile logic-in-memory," *IEEE J. Electron Devices Soc.*, vol. 8, pp. 748–756, 2020, doi: 10.1109/JEDS.2020.2987084.

[15] H. Mizuta, M. Wagner, and K. Nakazato, "The role of tunnel barriers in phase-state low electron-number drive transistors (PLEDTRs)," *IEEE Trans. Electron Devices*, vol. 48, no. 6, pp. 1103–1108, Jun. 2001.

[16] K.-D. Kim, K.-H. Lee, S.-J. Baik, J.-H. Lee, T.-K. Kim, and J.-T. Kong, "Characterization of multi-barrier tunneling diodes and vertical transistors using 2-D device simulation," in *Proc. Int. Conf. Simulation Semiconductor Processes Devices*, 2002, pp. 167–170.

[17] S. J. Ahn, G. H. Koh, K. W. Kwon, S. J. Baik, G. T. Jung, Y. N. Hwang, H. S. Jeong, and K. Kim, "Highly scalable and CMOS-compatible STTM cell technology," in *IEDM Tech. Dig.*, Dec. 2003, pp. 267–270.

[18] S. J. Baik, Z. Huo, S.-H. Lim, I.-S. Yeo, S. Choi, U.-I. Chung, and J. T. Moon, "STTM-promising nanoelectronic DRAM device," in *Proc. 4th IEEE Conf. Nanotechnol.*, Aug. 2004, pp. 45–46.

[19] K. Nakazato, K. Itoh, H. Ahmed, H. Mizuta, T. Kisu, M. Kato, and T. Sakata, "Phase-state low electron-number drive random access memory (PLEDM)," in *IEEE Int. Solid-State Circuits Conf. (ISSCC) Dig. Tech. Papers*, Feb. 2000, pp. 132–133.

[20] S. Kang, W. Y. Cho, B.-G. Choi, B. Cho, H.-R. Oh, H.-J. Kim, S.-J. Baik, D. Kim, C.-K. Kwak, and H.-G. Byun, "Scalable two transistor memory (STTM) for mobile embedded applications with 80nm technology," in *Proc. ISOCC*, 2004, pp. 159–162.

[21] W. Zhao and Y. Cao, "Predictive technology model for nano-CMOS design exploration," *ACM J. Emerg. Technol. Comput. Syst.*, vol. 3, no. 1, p. 1, Apr. 2007.

[22] *The International Technology Roadmap for Semiconductors*, ITRS, London, U.K., 2005.

[23] BSIM Group. (2011). *BSIM 4.7 Manual*. [Online]. Available: https://berkeley.edu

[24] P. Packan et al., "High performance 32 nm logic technology featuring 2nd generation high-k+ metal gate transistors," in *IEDM Tech. Dig.*, Dec. 2009, pp. 1–4.

SUEYEON KIM received the B.S. and M.S. degrees in electrical and electronics engineering from Konkuk University, Seoul, South Korea, in 2020 and 2023, respectively. Her research interests include logic-in-memory device and design technology co-optimization.

INSOO CHOI received the B.S. degree in electronic engineering from Konkuk University, Seoul, South Korea, in 2023. From 2021 to 2023, he was a Research Assistant with the Device Research Laboratory, Konkuk University. His research interest includes the development of device.

SANGKI CHO received the B.S. degree in electrical and electronic engineering from Konkuk University, Seoul, Republic of Korea, in 2023, where he is currently pursuing the M.S. degree in electrical and electronics engineering. His research interests include the next generation technology of semiconductor device and compact modeling.

MYOUNGGON KANG (Senior Member, IEEE) received the B.S. degree (Hons.) in electronics and information engineering from Chonbuk National University, Jeonju, in 2003, and the M.S. and Ph.D. degrees in electrical engineering from Seoul National University, Seoul, South Korea, in 2005 and 2012, respectively. He is currently an Associate Professor with the Department of Electronics Engineering, Korea National University of Transportation, Chungju, South Korea.

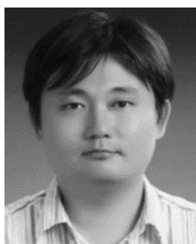

SEUNGJAE BAIK received the B.S., M.S., and Ph.D. degrees in electrical engineering from the Korea Advanced Institute of Science and Technology (KAIST), Daejeon, South Korea, in 1994, 1996, and 2001, respectively. From 2001 to 2009, he was with Samsung Electronics Company Ltd., Yongin, South Korea, where he contributed to novel Si devices, high-density flash memory devices, and charge trap flash memory devices, as a Senior Engineer and a Principal Engineer. From 2009 to 2012, he was with KAIST as a Research Professor, where he contributed to thin film Si solar cells, quantum dot solar cells, new memory materials, and devices. From 2012 to 2022, he was with Hankyong National University, Anseong-si, South Korea, as an Associate Professor. Since 2023, he has been a Master Engineer with the Samsung Research and Development Center, South Korea. His current research interests include charge trap memory devices, phase change memory devices, and plasma epitaxial growth.

CHANGHO RA received the B.S. and M.S. degrees in nano engineering from Sungkyunkwan University, Suwon, South Korea, in 2009 and 2018, respectively. From 2020 to 2023, he worked at Konkuk University Device Research lab, Seoul, South Korea. Since 2023, he has been joined Sungkyunkwan University, Device Research lab. His research interest includes design technology co-optimization.

JONGWOOK JEON received the B.S. degree in electrical engineering from Sungkyunkwan University, South Korea, in 2004, and the Ph.D. degree in electrical engineering from Seoul National University, Seoul, South Korea, in 2009. He was a Senior and Principal Engineer with the Samsung Research and Development Center, South Korea, from 2009 to 2017. From 2017 to 2023, he was an Assistant Professor and an Associate Professor with the Department of Electrical Engineering, Konkuk University, South Korea. Since 2023, he has been an Associate Professor with the School of Electronic and Electrical Engineering, Sungkyunkwan University. His research interest includes the design-technology co-optimization (DTCO) of next generation technology of semiconductor device.